ResearchGate

See discussions, stats, and author profiles for this publication at: https://www.researchgate.net/publication/13567800

Interaction Site for Soluble Cytochromes on the Tetraheme Cytochrome Subunit Bound to the Bacterial Photosynthetic Reaction Center Mapped by Site-Directed Mutagenesis †

ARTICLE *in* BIOCHEMISTRY · SEPTEMBER 1998

Impact Factor: 3.02 · DOI: 10.1021/bi980910h · Source: PubMed

CITATIONS
33

READS
14

7 AUTHORS, INCLUDING:

Artur Osyczka
Jagiellonian University
65 PUBLICATIONS **1,118** CITATIONS
SEE PROFILE

Satoshi Sogabe
Takeda Pharmaceutical Company Limited
28 PUBLICATIONS **724** CITATIONS
SEE PROFILE

Available from: Artur Osyczka
Retrieved on: 31 January 2016

Interaction Site for Soluble Cytochromes on the Tetraheme Cytochrome Subunit Bound to the Bacterial Photosynthetic Reaction Center Mapped by Site-Directed Mutagenesis†

Artur Osyczka,*,‡ Kenji V. P. Nagashima,‡ Satoshi Sogabe,§,|| Kunio Miki,§ Makoto Yoshida,‡ Keizo Shimada,‡ and Katsumi Matsuura‡

Department of Biology, Tokyo Metropolitan University, Minamiohsawa 1−1, Hachioji, Tokyo 192−03, Japan, and Department of Chemistry, Graduate School of Science, Kyoto University, Sakyo-ku, Kyoto 606-8502, Japan

Received April 21, 1998; Revised Manuscript Received June 11, 1998

ABSTRACT: The crystallographic structure of the *Blastochloris* (formerly called *Rhodopseudomonas*) *viridis* tetraheme cytochrome subunit bound to the photosynthetic reaction center (RC) suggests that all four hemes are located close enough to the surface of the protein to accept electrons from soluble cytochrome c_2. To identify experimentally the site of this reaction we prepared site-directed mutants of *Rubrivivax gelatinosus* RCs with surface charge substitutions in the bound cytochrome subunit and studied the kinetics of their reduction by soluble cytochromes (mitochondrial horse cytochrome *c*, *Blc. viridis* cytochrome c_2, and *Rvi. gelatinosus* cytochrome c_8). In comparison with the wild-type, the mutants E79K (glutamate-79 substituted by lysine), E93K (glutamate-93 substituted by lysine), and E85K (glutamate-85 substituted by lysine) located near the solvent-exposed edge of low-potential heme 1, the fourth heme from the special pair of bacteriochlorophyll, exhibited decreased second-order rate constants for the reaction between the tetraheme subunit and the soluble cytochromes. Double charge substitutions in this region: E79K/E85K (glutamate-79 and -85 both replaced by lysine) and E93K/E85K (glutamate-93 and -85 both replaced by lysine) appeared to show an additive inhibitory effect. Mutations in other charged regions did not alter the kinetics of electron transfer between bound and soluble cytochromes. In light of the available structural information on *Blc. viridis* RC, these results indicate that the cluster of acidic residues immediately surrounding the distal heme 1 of the RC-bound tetraheme subunit forms an electrostatically favorable binding site for soluble cytochromes. Thus, all four hemes in the subunit seem to be directly involved in the electron transfer toward the photo-oxidized special pair of bacteriochlorophyll. On the basis of these findings, a model is proposed for the hypothetical cytochrome c_2−RC transient complex for *Blc. viridis*.

After the three-dimensional structures of photosynthetic reaction centers (RCs)[1] were solved to high resolution in two species of purple bacteria, *Blastochloris* (formerly called *Rhodopseudomonas*, ref *1*) *viridis* (*2*−*4*) and *Rhodobacter sphaeroides* (*5*−*7*), further studies of the structure−function relationships of this photosynthetic protein complex became possible using site-specific mutagenesis. A prerequisite for such experiments is the existence of efficient gene-transfer systems, which however are not always accessible since various species of purple bacteria respond differently to genetic treatment. *Rba. sphaeroides* and *Rhodobacter capsulatus* are well-known to be amenable to genetic manipulations and are thus widely used in the construction of site-directed mutants of RCs (for reviews see refs *8*, *9*). These two species possess an RC without a bound tetraheme cytochrome subunit and are capable of grow under both photosynthetic and aerobic conditions. In this respect they differ from most species of purple bacteria which contain an RC with bound cytochrome, and where inability to carry out aerobic respiration is a limiting factor in performing genetic manipulations. In the latter group, a transformation protocol has been developed solely for *Blc. viridis* (*10*), so far providing a limited number of site-specific mutants restricted to the L and M subunits (*10*−*13*). Point mutations in the bound cytochrome subunit have not yet been reported, leaving many questions related to the mechanisms of electron transfer within this subunit still unanswered.

The hemes of the bound cytochrome act as reductants for the photo-oxidized special pair of bacteriochlorophyll (P), and are subsequently re-reduced by soluble proteins mediating electron transfer from the cytochrome bc_1 complex to

† This work was supported in part by a grant-in-aid from the Ministry of Education, Science and Culture, Japan (0904423 and the Decoding the Earth Evolution Program).

* Corresponding author. Phone: (81) (426) 77 2582. Fax: (81) (426) 77 2559. E-mail: artur@comp.metro-u.ac.jp.

‡ Tokyo Metropolitan University.

§ Kyoto University.

|| Present address: Nippon Roche Research Center, Department of Chemistry, Kajiwara 200, Kamakura, Kanagawa 247-8530, Japan.

[1] Abbreviations: *Blc.*, *Blastochloris*; *Rba.*, *Rhodobacter*; *Rvi.*, *Rubrivivax*; *Rfx.*, *Rhodoferax*; *Rcy.*, *Rhodocyclus*; *Rsp.*, *Rhodospirillum*; RC, reaction center; HiPIP, high-potential iron−sulfur protein; E_m, redox midpoint potential; P, special pair of bacteriochlorophyll; DAD, 2,3,5,6-tetramethylphenylenediamine; PCR, polymerase chain reaction; bp, base pair; kb, kilo base pair; E79K, E85K, E93K, E112K, and E197K, glutamate-79, -85, -93, -112, and -197 substituted with lysine, respectively; D46H and D276H, aspartate-46 and -276 substituted with histidine, respectively; E79K/E85K, glutamate-79 and -85 substituted with lysines; E93K/E85K, glutamate-93 and -85 substituted with lysines.

S0006-2960(98)00910-6 CCC: $15.00 © 1998 American Chemical Society
Published on Web 08/01/1998

the RC (*14, 15*). Although kinetic studies, redox potentiometry, and genetic analysis have provided a considerable amount of information concerning the structure and properties of tetraheme subunits in various species, relatively little is known about the interaction with their electron-donating partners. Although electron transfer from soluble, periplasmic electron carriers (cytochrome c_2 in many species, or alternatively, high-potential iron−sulfur protein (HiPIP) and cytochrome c_8, as recently reported for some species from the β-subclass (*16*−*20*)) to the photo-oxidized tetraheme subunit has been well-characterized, the location of the docking site for these proteins on the surface of tetrahemic cytochrome remains undefined.

The three-dimensional structure of *Blc. viridis* RC shows that all four hemes in the subunit are situated close enough to the surface to accept electrons carried by mobile mediators (*2*−*4*). Experimental evidence also exists indicating that the binding of soluble cytochromes to the RC is guided by attractive electrostatic interactions (*21*−*23*). This allowed the assumption to be made that a putative docking site on the surface of the tetraheme subunit is formed by negatively charged carboxylate groups surrounding a solvent-exposed heme edge, which may interact electrostatically with lysine residues surrounding the heme crevice of cytochrome c_2. Although this has not been experimentally verified, three possible, electrostatically suitable regions located near exposed edges of low-potential heme 1 (*c*-554), high-potential heme 2 (*c*-556), and high-potential heme 3 (*c*-559) have been predicted from the crystallographic structure of *Blc. viridis* tetraheme subunit (*21, 22, 24*).

From time-resolved optical spectroscopy, these positions are difficult to distinguish mainly due to rapid electron exchange between individual hemes within the cytochrome subunit compared to electron transfer from soluble components. The time constants for the reaction between soluble electron carriers and the tetraheme subunit (range of milli- to microseconds) are in many cases at least 1 order of magnitude slower than the time constants for the interheme electron transfer within the subunit (range of micro- to nanoseconds). Therefore, the intrasubunit heme−heme electron transfer following reaction with a soluble electron donor makes it difficult to detect the heme which directly accepts the electron. The docking site can, however, be mapped experimentally by introducing point mutations which aim to alter specifically the local surface charge of the tetraheme subunit, with the assumption that the electrostatically controlled interaction with a soluble electron donor will be affected, if altered positions participate in the binding.

Addressing this question in our experimental approach, we established a new genetic system suited for site-directed mutagenesis of the RC-bound tetraheme cytochrome subunit of *Rubrivivax gelatinosus*, a species that seemed appropriate for this purpose for several reasons. Unlike most of the bacterial species having the RC-bound tetraheme subunit, *Rvi. gelatinosus* can easily grow under both photosynthetic and respiratory conditions. Its *puf* operon, containing the photosynthetic genes coding for the RC subunits, has been sequenced and well-characterized for two strains: IL144 (*25*) and S1 (*26, 27*). Its tetraheme cytochrome subunit shows a high degree of similarity in amino acid sequence with the *Blc. viridis* tetraheme subunit (*25*). Redox midpoint potentials and α-band absorption wavelengths of four hemes of the *Rvi. gelatinosus* cytochrome subunit, as well as the geometry of their arrangement with respect to the membrane plane, have already been determined (*28, 29*). The gene-transfer system has already been successfully applied to inactivate the *puf*C gene in strain IL144, providing a photosynthetically competent C244 mutant without the bound cytochrome subunit (*30*). Various *puf* deletion mutants in *Rvi. gelatinosus* strain S1 were also engineered through gene-transfer techniques (*27, 31, 32*).

In this work, we describe a new gene-transfer system for *Rvi. gelatinosus*, which is based on a homologous recombination between genomic DNA of a newly constructed ΔC mutant lacking the original copy of the bound cytochrome gene on the chromosome and a nonreplicative plasmid bearing the mutated copy of this gene. This system was applied to generate the first site-specific mutants of the RC-bound cytochrome subunit. All mutants have charged amino acid substitutions located on the surface of the protein in proximity to the exposed edges of hemes considered as possible direct acceptors of electrons from soluble electron donors. Single mutants E79K, E85K, E93K, E112K, and E197K (glutamate-79, -85, -93, -112, and -197 replaced by lysines) and D46H and D276H (aspartate-46 and -276 replaced by histidines) were prepared in order to define the area of the surface of the cytochrome subunit involved in the recognition of soluble cytochromes and to evaluate the electrostatic contribution of individual charged amino acids to protein−protein association. Double charge substitutions E79K/E85K (glutamate-79 and -85 to lysines) and E93K/E85K (glutamate-93 and -85 to lysines) were designed to test for additive electrostatic effects in the identified interaction domain.

MATERIALS AND METHODS

Construction of Plasmid for Deletion of the Cytochrome Subunit. The genes encoding for the RC proteins of *Rvi. gelatinosus* IL144 have been cloned and described previously (*25*). The gH3 plasmid (a derivative of pUC118 containing the genes for M and C subunits and a 1.7-kb downstream region of the *puf* operon) was digested at the unique *Sac*I site (polycloning site) and the *Sph*I site within the cytochrome gene (partial digestion) to excise a 2.7-kb fragment (downstream of *Sph*I site) containing the major part of the cytochrome gene (for positions of restriction sites see Figure 1a). The remaining part of this gene (114 bp) was removed through digestion with *Xba*I and *Sph*I (polycloning site) followed by Exonuclease III treatment (Kilo sequence deletion kit, Takara Shuzo Co., Ltd.). This manipulation was necessary due to the lack of suitable restriction site between *puf*M and *puf*C which is required for correct excision of *puf*C from gH3. The elimination of the gene for the cytochrome subunit in the resulting clones was screened by DNA sequence analysis and plasmid gHMC13 containing the entire *puf*M, and 13 bp from the start of *puf*C was used in the subsequent construction of gHMKD (see below).

A 1.7-kb *Not*I fragment from gH3 (downstream region of *puf* operon containing a part of the *crt*D gene) was treated with T4 DNA polymerase to create blunt ends and inserted into the *Xho*I site of pUCKM1 bearing a kanamycin resistance cartridge (Km^r) (*33*). The correct orientation of the insert in the resulting pUCKD1 plasmid was checked

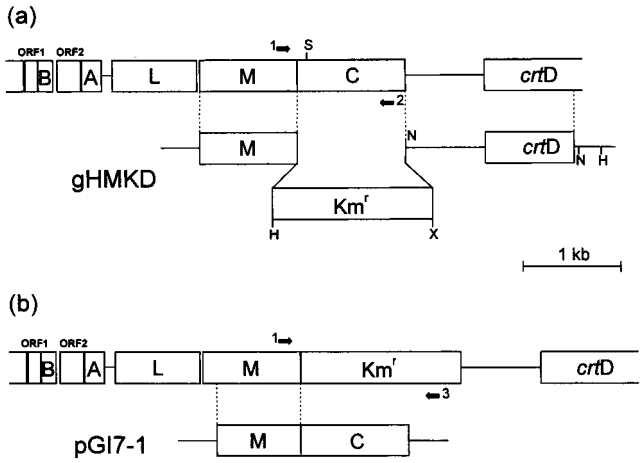

FIGURE 1: Scheme for the homologous recombination events yielding *Rvi. gelatinosus* mutated strains: (a) double crossover recombination between the genome of the wild-type IL144 strain and the plasmid gHMKD to obtain the ΔC mutant and (b) complementation of the ΔC mutant with the plasmid pGI7-1 to generate the wild-type phenotype or RC site-specific mutants. Both gHMKD and pGI7-1 are pUC derived plasmids and bear the ampicillin resistance gene. The rectangles represent the photosynthetic genes of the *puf* operon coding for L, M, and cytochrome subunits of the RC (L, M, and C, respectively) and the α and *β* subunits of the B870 light-harvesting complex (A and B, respectively); *crt*D, carotenoid gene; ORF, open reading frame; Km^r, kanamycin resistance cartridge. Positions of restriction sites used in the construction of gHMKD are the following: S, *Sph*I; H, *Hind*III; N, *Not*I; X, *Xho*I. Arrows indicate positions of oligonucleotides used as primers 1, 2, and 3 in PCRs of genomic DNAs.

by endonuclease restriction mapping. A 3.6-kb *Hind*III fragment from pUCKD1 containing the Km^r gene and the 1.7-kb downstream region of the *puf* operon was ligated into gHMC13 at the *Hind*III site to give the final construct gHMKD (Figure 1a), which was electroporated into *Rvi. gelatinosus* IL144 cells.

Electroporation and Selection of ΔC Mutant. Rvi. gelatinosus IL144 cells were prepared for electroporation from photosythetically grown cultures as described previously (*30*). Forty microliters of cell suspension mixed with 1 μg of gHMKD plasmid DNA was electroporated in a 2-mm gap cuvette using the ECM 600 system (BTX, San Diego, CA). The resistance was set at 246 Ω and the field strength at 12.5 kV/cm, generating a pulse length of approximately 12 ms. Immediately after electroporation, cells were chilled on ice in 1 mL of 1% glucose PYS medium (0.5% polypeptone, 0.1% yeast extract, 0.5% sodium succinate, and minerals, pH 7.0), transferred to 10 mL of 1% glucose PYS medium, and incubated at 30 °C in darkness, overnight. A 2-mL aliquot of the culture was added to 100 mL of PYS medium containing 50 μg/mL kanamycin and grown aerobically at 30 °C. Kanamycin-resistant colonies were maintained on PYS plates (50 μg/mL kanamycin), propagated on PYS medium (50 μg/mL kanamycin), and then transferred to PYS plates containing 50 μg/mL ampicillin. Ampicillin-sensitive transformants were isolated.

Complementation of ΔC Mutant to RC−Wild-Type and Site-Specific Mutants. Site-directed mutagenesis was performed on the basis of the Kunkel method, using the Mutan-K mutagenesis kit (Takara Shuzo Co., Ltd.). The pGI7-1 plasmid (pUC118 encompassing 0.85-kb fragment of *puf*M and entire *puf*C) (*25*) was used as template DNA (Figure 1b). The sequences of mismatch oligonucleotides used to introduce single-point mutations are listed in Table 1. Double-point mutations E93K/E85K and E79K/E85K were constructed from the template containing E85K, using the same oligonucleotides as for respective single mutants. Mutations and the sequence integrity of the *puf*C gene were further confirmed by DNA sequence analysis (Applied Biosystems 373A DNA Sequencer). *Rvi. gelatinosus* ΔC mutant cells were electroporated with unchanged or mutated pGI7-1 plasmids as described above. Transformant cells were selected on PYS medium containing 50 μg/mL ampicillin following the strategy used to select the ΔC mutant, and clones derived from single colonies were taken for further analysis.

Table 1: Oligonucleotides Used for Site-Directed Mutagenesis

mutation	oligonucleotide sequence[a]
D46H	5′-CCGAGTTGTGGGCCACCGGCGT-3′
E79K	5′-CCACCCATTTG*GT*GATCGCCGCCA-3′ [b]
E85K	5′-TAGTTGCAGCCCTTGGTCGGCG-3′
E93K	5′-GGCCAGGTTCTTGGTATGGCAGT-3′
E112K	5′-TCTGCGTCATCTTGAGCATCCGG-3′
E197K	5′-CGGACGTTCGTCTTTTCCTTCAG-3′
D276H	5′-TTGTTGTTGAGGTGACGCGCCATG-3′

[a] Mismatch positions are underlined. [b] Italic indicates a correction to the sequence from ref *25*.

Genetic Analysis of Mutated Strains. Genomic DNA from wild-type and mutants of *Rvi. gelatinosus* was isolated and purified as described previously (*30*). One microgram of DNA was blotted on a Hybond-N nylon membrane (Amersham, UK) and hybridized with a ^{32}P-labeled kanamycin resistance cartridge, pUC118, or a 0.7-kb *Apa*I fragment of the gene coding for the cytochrome subunit according to a manual on DNA manipulation (*34*). The 1.2-kb DNA fragments of *puf*C gene were amplified from genomic DNAs through polymerase chain reaction (PCR) with the use of the following set of oligonucleotides: 5′-GCCCAGCTGTTCTGGGTCGG-3′ (primer 1; at the 3′ end of *puf*M, −233 bp from *puf*C) and 5′-CGGCTTGTAGGCACCCTGGTGGCA-3′ (primer 2; at the 3′ end of *puf*C, 956 bp from the start codon). The 1.6-kb fragment containing a part of *puf*M and the Km^r gene was amplified from genomic DNA of the ΔC strain, with the use of primer 1 (as described above) and 5′-TCCGCGAGGTCGTCCAGCC-3′ (primer 3; at the 3′ end of the Km^r gene). The positions of primers 1−3 are shown in Figure 1. PCR reactions carried out using Zymoreactor (ATTO, Japan) consisted of 30 cycles of 1 min at 94 °C, 30 s at 65 °C, and 2 min at 72 °C. When site-directed mutants were examined, amplified PCR fragments were purified on MicroSpin S-400 HR columns (Pharmacia LKB) and subjected to DNA sequence analysis in order to confirm the presence of introduced mutations in the genomic DNA of the mutated strains.

Preparation of Membrane Fractions and Proteins. Membrane fractions containing the RC complexes from photosynthetic cultures of wild-type (grown on PYS medium) or mutant (grown on PYS containing 50 μg/mL ampicillin) strains of *Rvi. gelatinosus* were collected from cell homogenates by differential centrifugation as described previously (*35*), washed twice in 5 mM Tris-HCl pH 8, centrifuged, and finally suspended in the same buffer. Cytochrome c_8 and HiPIP were prepared from the remaining supernatant as

reported (*35*). Cytochrome c_2 was purified from *Blc. viridis* according to established procedures (*36*). Horse heart mitochondrial cytochrome *c* (type VI) was obtained from Sigma.

Kinetic Spectrophotometry. Xenon-flash-induced absorbance changes of cytochromes were recorded using a single-beam spectrophotometer as described previously (*37*). Experiments were performed aerobically in 5 or 10 mm path length cuvettes with 2 mM Tris-HCl (pH 8) containing 20 μM DAD and sodium ascorbate (0.2 mM for horse cytochrome *c* and *Blc. viridis* cytochrome c_2, 2 mM for *Rvi. gelatinosus* cytochrome c_8). Second-order rate constants for the reaction between the RCs and soluble cytochromes were determined from measurements conducted under pseudo-first-order conditions (much higher concentrations of cytochromes with respect to the concentration of RCs). In typical experiments, cytochromes were used at the following concentrations: 40 μM, horse cytochrome *c*; 60 μM, *Blc. viridis* cytochrome c_2; 4 μM, *Rvi. gelatinosus* cytochrome c_8. The concentration of membranes was adjusted to $A_{850} = 1.0$ (approximately 0.1 μM RC). The reduction of bound cytochrome and the oxidation of soluble cytochromes were followed by monitoring at wavelengths of 556 and 548 nm, respectively.

Model Building and Electrostatic Calculations. The model of the cytochrome subunit of the *Rvi. gelatinosus* RC based on the sequence alignment described in ref *38* and the coordinates of the *Blc. viridis* RC (protein data bank entry 1PRC) was built by adopting the following procedure. An initial model, with amino acids of *Rvi. gelatinosus* subunit superimposed onto the *Blc. viridis* structure, was manually built using the programs X-UTIL (*39*) and O (*40*). This structure was then refined by a simulated annealing and molecular dynamics protocol using the program X-PLOR (*41*) to obtain reasonable stereochemical parameters. The quality of the resulting model was examined using the program PROCHECK (*42*). All irregularities observed during the modeling procedures were analyzed in detail and subjected to further refinement with additional or modified restraints.

The analysis of the electrostatic potentials of the RC-bound tetraheme subunit and cytochrome c_2 has been performed by calculating the electrostatic potential surfaces of their models with the use of the program GRASP (*43*).

In modeling the hypothetical cytochrome c_2−RC binding site structural factors (for instance, salt linkages, van der Waals contacts, and electrostatic potentials) were considered in order to maximize favorable interactions and exclude steric conflicts by manual adjustment. In addition, cytochrome c_2 and the RC were mutually orientated to minimize the distance between solvent-exposed atoms of the prosthetic groups. Some reorientations of side chains involved in intermolecular salt linkages were allowed in order to optimize their interaction geometry. Finally, interatomic distances were checked to ensure that no van der Waals overlap occurred between atoms at the intermolecular interface.

RESULTS

Preparation of Mutants of Bound Cytochrome Subunit. *Rvi. gelatinosus puf*C deletion mutant (ΔC) was constructed through double crossover recombination between wild-type genomic DNA and the pUC-based gHMKD plasmid containing a kanamycin resistance cartridge flanked by sequences homologous to *puf*M (1 kb) and the 1.7-kb downstream region of *puf*C (Figure 1a). After electroporation of IL144 wild-type cells with gHMKD, a single crossover recombinant C1 strain was initially selected using the kanamycin resistance (Km^r) marker. Although the wild-type strain is ampicillin-sensitive, the C1 strain was ampicillin-resistant, indicating that the entire gHMKD was incorporated into genomic DNA. Several nonselective transfers of the C1 strain enabled us to select a kanamycin-resistant and ampicillin-sensitive ΔC mutant bearing the characteristics of a double crossover recombinant. Southern blot analysis (Figure 2) of genomic DNA purified from the ΔC strain confirmed the deletion of *puf*C and its replacement with a kanamycin resistance cartridge (ΔC exhibited a positive signal against the Km^r gene, but not against pUC and the *puf*C gene). In further PCR analysis, the combination of oligonucleotides designed to selectively amplify *puf*C (Figure 1a; primers 1 and 2) resulted in the amplification of a 1.2-kb product only in the wild-type and C1, but not in ΔC, providing additional confirmation of the deletion of *puf*C from the *puf* operon in the ΔC mutant (data not shown). The location of the Km^r gene immediately downstream of *puf*M in the chromosome of the ΔC mutant was also confirmed by DNA sequence analysis of the 1.6-kb fragment containing the 3′ end of *puf*M and a major part of the Km^r gene amplified from genomic DNA with the use of primers 1 and 3 (Figure 1b). As expected, the ΔC mutant shared a phenotype with the previously constructed and characterized C244 *Rvi. gelatinosus* mutant (*30*): the capability to grow under both aerobic respiratory and anaerobic photosynthetic conditions, the absence of bound cytochrome in membrane preparations, and a significantly slower growth rate under photosynthetic conditions as compared to the wild-type.

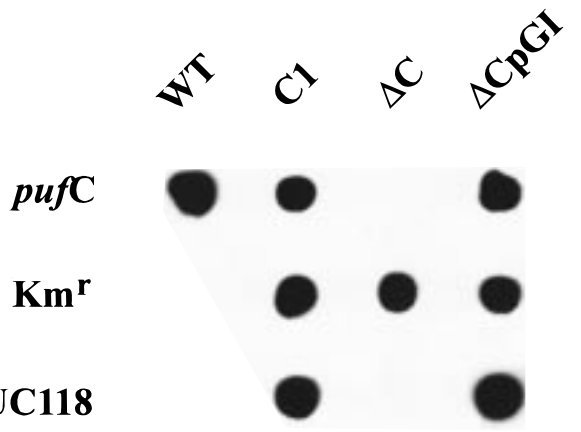

FIGURE 2: Southern blot analysis of genomic DNAs of wild-type and mutated strains of *Rvi. gelatinosus*. Each dot contained genomic DNA purified from a strain shown in the upper area of the figure. The genes used as probes are represented on the left side.

The ΔC mutant was used as a deletion background for further experiments, which aimed to restore the correct structure of the entire *puf* operon by a single crossover recombination between the chromosome and the complementing plasmid (Figure 1b). Such transformants were obtained by electroporation of the ΔC mutant cells with the nonreplicative plasmid pGI7-1, which contained all *puf*C and a 0.85-kb fragment homologous to *puf*M cloned into pUC118. Recombinant cells (ΔCpGI strain) were selected

with the use of an ampicillin resistance marker. The correct insertion of *puf*C into the chromosome of ΔCpGI was confirmed by Southern blot analysis (Figure 2) and the presence of a 1.2-kb product, containing *puf*C, amplified by PCR. The ΔCpGI strain regained the wild-type phenotype, expressing the RCs with the bound tetraheme subunit and exhibiting a growth rate under photosynthetic conditions which was equal to that of the wild-type.

To prepare site-specific mutants in the *puf*C gene, copies of mutated pGI7-1 were used to complement the ΔC deletion background. Point mutations introduced in pGI7-1 were successfully incorporated into the chromosome of ΔC cells, generating the mutants with site-specific alterations in the RC-bound cytochrome subunit. For each mutant obtained, DNA sequence analysis of *puf*C amplified from genomic DNA through PCR confirmed the presence of the desired mutation. All introduced mutations did not alter the level of expression of RCs or the photosynthetic growth rates of the cells (which were comparable with those of the wild-type).

Electron Transfer Between Soluble Cytochromes and Mutants of Bound Cytochrome Subunit. Kinetic traces for the reaction of mitochondrial cytochrome *c* with wild-type and mutants of the bound cytochrome subunit presented in Figure 3 show the flash-induced photo-oxidation of bound cytochrome (downward signal at 556 nm) followed by its re-reduction (absorbance increase at 556 nm) with concomitant oxidation of soluble cytochrome (absorbance decrease at 548 nm). Mutated positions were: E79, E85, E93, and D46 near low-potential heme 1; E85, E112, and D276 near high-potential heme 2; and E197 near high-potential heme 3. It can be clearly recognized that mutations at positions E112, E197, and D276 in bound cytochrome did not change the kinetics of its reduction by soluble cytochrome (Figure 3b−d), in contrast to the mutants at positions D46, E85, E79, and E93 (Figure 3e−h) which were reduced with significantly decreased rates relative to the wild-type (second-order rate constants for these reactions are shown in Table 2). The extent of inhibition was site-specific giving the following order of reactivity: wild-type > D46H > E85K > E79K, E93K. Moreover, double-charge substitutions E79K/E85K and E93K/E85K resulted in additive electrostatic inhibition as compared to the single-charge substitutions at position E79, E93, or E85 (Figure 3i,j; Table 2).

In Figure 4, the second-order rate constants for the wild-type, the single mutants at positions D46, E85, E79, and E93, and the double mutants are plotted as a function of ionic strength. The mutants exhibit a decrease in rate constants with increasing ionic strength in a manner similar to that of the wild-type, indicating that oppositely charged residues substituted at these positions do not eliminate electrostatic attractions in the cytochrome−RC transient complex.

Applying the parallel plate (Watkins) electrostatic model for protein−protein interactions (*44*, *45*), the experimental data were fitted to the following equations:

$$\ln k(\mathrm{I}) = \ln k_{\infty} - V_{\mathrm{ii}} X(\mathrm{I}) \qquad (1)$$

$$X(\mathrm{I}) = (1 + 0.33\,\mathrm{I}^{1/2}R)^{-1} \exp(-0.33\,\mathrm{I}^{1/2}R) \qquad (2)$$

where $k(\mathrm{I})$, k_{∞}, and R are the second-order rate constant at a given ionic strength, the second-order rate constant at infinite ionic strength, and the radius of the interaction site, respectively. From the value of the parameter V_{ii}, the electrostatic interaction energy (V_{TOT}) can be calculated as $V_{\mathrm{TOT}} = kTV_{\mathrm{ii}}$ (*44*).

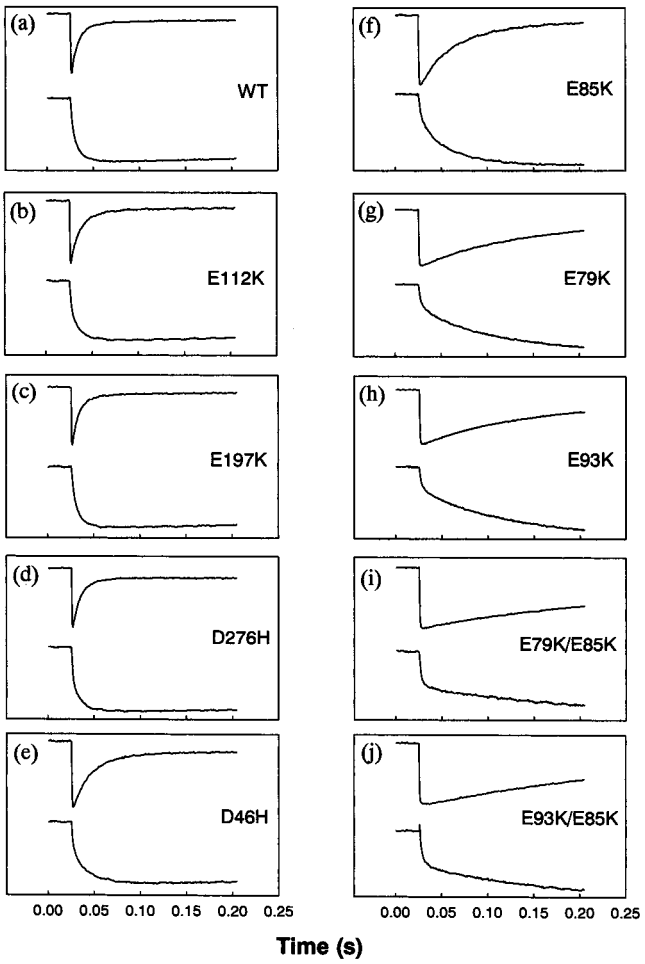

FIGURE 3: Single-flash kinetics for the reaction of wild-type (a) and mutant (b−j) tetraheme subunits of *Rvi. gelatinosus* RC with 40 μM horse mitochondrial cytochrome *c*. Upper and lower traces in each panel represent absorbance transients at 556 and 548 nm, respectively. The height of each panel corresponds to ΔABS of 3.5×10^{-3}. All traces are plotted on the same time resolution scale. Experimental conditions were as described in Materials and Methods.

The best fit of the experimental data for wild-type RCs yields the value $R = 10.4$ Å and the interaction energy $V_{\mathrm{TOT}} = -3.2$ kcal/mol (Table 2). The values of the energy term estimated for mutant RCs (shown in Table 2) indicate that residues E79, E93, and E85 are involved in the electrostatic recognition of soluble cytochrome (less energetically favorable complexes yield higher values as compared to that of the wild-type). The largest increase of 2.0 kcal/mol observed for mutants E79K and E93K suggests that E79 and E93 form the strongest electrostatic interactions in the cytochrome *c*−RC transient complex. The effect is smaller for mutant E85K (increase of 1.0 kcal/mol), but still large enough to suggest the involvement of E85 in the binding of cytochrome *c*. The V_{TOT} value estimated for double mutants E79K/E85K and E93K/E85K (−0.5 kcal/mol), being higher than V_{TOT} for single mutants E79K and E93K (−1.2 kcal/mol) and E85K (−2.2 kcal/mol), shows the additivity of the electrostatic effects in the cytochrome interaction domain. The small change observed for mutant D46H (increase in V_{TOT}

Table 2: Electrostatic Parameters Based on the Ionic Strength Dependence of the Second-Order Rate Constant (k) for the Reaction of Horse Mitochondrial Cytochrome *c* with Wild-Type and Mutants of *Rvi. gelatinosus* RC-Bound Tetraheme Subunit

RC	k ($M^{-1}s^{-1}$)[a]	k_∞ (M^{-1} s^{-1})	V_{TOT} (kcal/mol)	Z_{RC}	Z_{cyt}
WT[b]	4.5×10^6	6.1×10^4	−3.2	−3.6	+3.6
E112K	4.1×10^6	6.8×10^4	−3.2	−3.6	+3.6
E197K	4.5×10^6	6.2×10^4	−3.3	−3.7	+3.6
D276H	4.4×10^6	6.6×10^4	−3.2	−3.6	+3.6
D46H	2.2×10^6	6.5×10^4	−2.6	−3.0	+3.6
E85K	1.1×10^6	5.3×10^4	−2.2	−2.5	+3.6
E79K	3.3×10^5	5.5×10^4	−1.2	−1.4	+3.6
E93K	3.5×10^5	5.7×10^4	−1.2	−1.3	+3.6
E79K/E85K	1.1×10^5	5.6×10^4	−0.5	−0.6	+3.6
E93K/E85K	1.2×10^5	6.0×10^4	−0.5	−0.6	+3.6

[a] Measured in 2 mM Tris-HCl, pH 8. [b] RCs from recombinant ΔCpGI cells displayed the same kinetic behavior as those from the wild-type IL144 strain. The rate constant at infinite ionic strength (k_∞), the electrostatic interaction energy ($V_{TOT} = kTV_{ii}$), and the number of charges on the interaction domains of the RC (Z_{RC}) and soluble cytochrome (Z_{cyt}) were calculated by applying the parallel plate (Watkins) electrostatic model for protein−protein interactions (*44*) as described in the text.

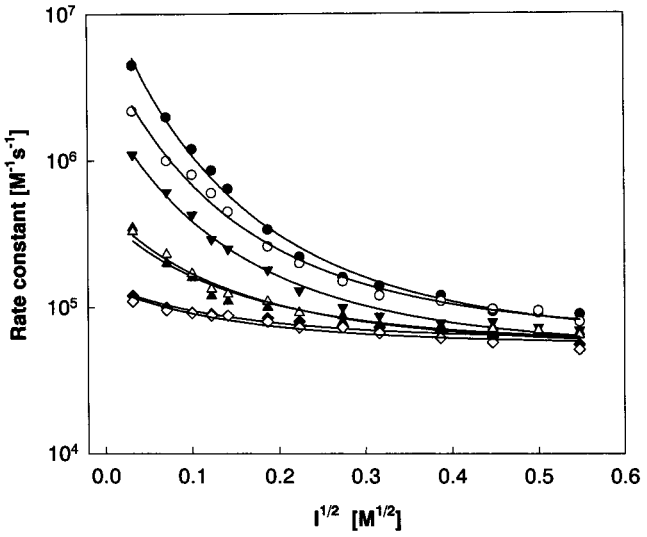

FIGURE 4: Ionic strength dependence of the observed second-order rate constants for the reaction of horse mitochondrial cytochrome *c* with wild-type and mutant tetraheme subunits of *Rvi. gelatinosus* RC. Symbols represent the values for the following: (●) wild-type; single mutants, (○) D46H, (▼) E85K, (△) E79K, (▲) E93K; double mutants, (◇) E79K/E85K, (◆) E93K/E85K. The solid lines correspond to fits of the data to eqs 1 and 2, as described in the text.

of 0.6 kcal/mol) suggests that this residue is located in a peripheral region of the binding site for soluble cytochrome *c*. In the latter mutant a His (not Lys) substitution may result only in a change of one charge at pH 8, which may partially account for the smaller effect, as compared to E79K, E93K, and E85K mutants where positive charges replace negative ones. The ionic strength dependency for the mutants which do not change the rates of reaction at low ionic strength (E112K, E197K, and D276H) was comparable to that observed for the wild-type (data not shown) yielding similar values of the interaction energy (Table 2).

The rate constants extrapolated to infinite ionic strength (where electrostatic effects are minimized) can be interpreted as reflecting the degree of structural perturbation caused by individual mutations (*45*). As shown in Table 2, k_∞ values for the wild-type and all mutants are similar, indicating that these mutations did not introduce significant perturbation in the heme environment other than altering local surface charges.

The product of the charges at the cytochrome *c*−RC interaction domain can be calculated from the equation $V_{ii} = \alpha Z_{RC} Z_{cyt} r_{12}/DR^2$, where $\alpha = 128.5$, Z_{RC} and Z_{cyt} are the charges on the interaction domains of the RC and soluble cytochrome, respectively, r_{12} is the distance between the surfaces of interacting molecules (taken as 3.5 Å for van der Waals contacts), and D is the effective dielectric constant at the interaction site (*44, 46*). Using $D = 10$ (in the case of partial exclusion of water molecules) and $R = 10.4$ Å, a value of $Z_{RC}Z_{cyt}$ estimated for the wild-type suggests three or four specific ionic pairs between cytochrome *c* and the tetraheme subunit (Table 2: $Z_{RC} = -3.6$, $Z_{cyt} = +3.6$). It should be noted that these values are in good agreement with the estimations reported for the reaction between soluble cytochromes and *Blc. viridis* RC-bound cytochrome subunit (*21, 22*). As shown in Table 2, in the interaction domains of some of the mutated cytochrome subunits (at positions D46, E85, E79, and E93), the number of charges decreased by 0.6 to 2.3/substituted residue. Assuming different extents of contribution of these positions in the binding of cytochrome, observed changes are within the range of decrease expected for the applied type of mutational substitutions and are consistent with the values reported elsewhere for similar types of cytochrome interactions (*45*).

Blc. viridis cytochrome c_2 was a poorer electron donor to *Rvi. gelatinosus* tetraheme subunit than horse cytochrome *c*, as demonstrated by the kinetic traces presented in Figure 5a (the second-order rate constant for this reaction was 3×10^5 M^{-1} s^{-1}). Nevertheless, when mutated tetraheme subunits were substituted for the wild-type in the reaction with *Blc. viridis* cytochrome c_2, the inhibitions caused by individual mutations were comparable to those observed for horse cytochrome *c* (Figure 5b−d shows representative kinetic traces). Mutants E79K, E93K, E85K, and D46H reacted with cytochrome c_2 with decreased rate constants relative to that of the wild-type, whereas mutants E112K, E197K, and D276H showed no changes in electron-transfer kinetics. Furthermore, as in the case of horse cytochrome *c*, mutations E93K and E79K had larger inhibitory effects than mutations E85K and D46H (the rate constants were 7×10^4 M^{-1} s^{-1} for the reaction with E93K and E79K and 1×10^5 M^{-1} s^{-1} for the reaction with E85K and D46H).

Cytochrome c_8, which is one of the physiological partners for the RC from *Rvi. gelatinosus*, reacted with the tetraheme subunit more efficiently than mitochondrial cytochrome *c*

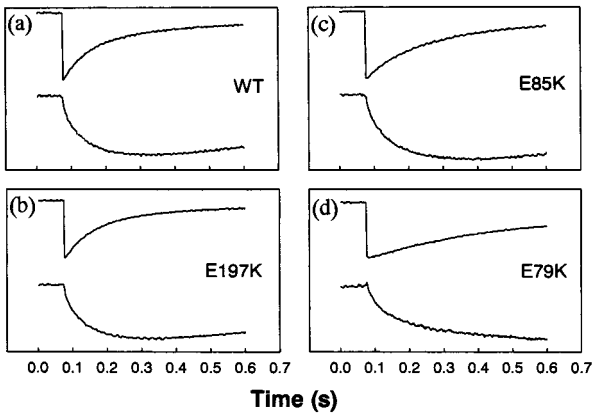

FIGURE 5: Single-flash kinetics for the reaction of wild-type (a) and mutant (b−d) tetraheme subunits of *Rvi. gelatinosus* RC with 60 μM *Blc. viridis* cytochrome c_2. Upper and lower traces in each panel represent absorbance transients at 556 and 548 nm, respectively. The height of each panel corresponds to ΔABS of 3.0×10^{-3}. All traces are plotted on the same time resolution scale. Experimental conditions were as described in Materials and Methods.

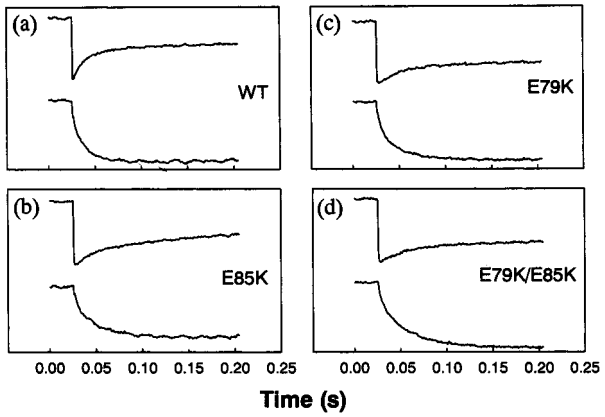

FIGURE 6: Single-flash kinetics for the reaction of wild-type (a) and mutant (b−d) tetraheme subunits of *Rvi. gelatinosus* RC with 4 μM *Rvi. gelatinosus* cytochrome c_8. Upper and lower traces in each panel represent absorbance transients at 556 and 548 nm, respectively. The height of each panel corresponds to ΔABS of 2.5×10^{-3}. All traces are plotted on the same time resolution scale. Experimental conditions were as described in Materials and Methods.

and *Blc. viridis* cytochrome c_2 and obeyed second-order kinetics with a rate constant of 3×10^7 M^{-1} s^{-1} (Figure 6a). Although it is not clear why the biphasic kinetics were obtained at 556 nm, the first millisecond phase corresponded well to the oxidation of cytochrome c_8 at 548 nm, and was thus analyzed. The electron donation from cytochrome c_8 was affected by individual mutations of the tetraheme subunit in a manner consistent with that observed for the other soluble cytochromes. Again, mutations at positions E79, E85, and E93 inhibited the electron-transfer kinetics indicating the decreased stability of the cytochrome c_8−RC transient complex (Figure 6b−d shows representative kinetic traces). Double mutations (E79K/E85K and E93K/E85K) showed larger inhibitory effects. The reaction of cytochrome c_8 with mutants E79K, E85K, and E93K occurred with the rate constant of 1.5×10^7 M^{-1} s^{-1}, whereas E79K/E85K and E93K/E85K reacted with the rate constant of 9×10^6 M^{-1} s^{-1}. Mutations in other regions, E112K, E197K, and D276H, as in the case of the other cytochromes, did not inhibit the electron transfer from cytochrome c_8.

When *Rvi. gelatinosus* HiPIP was assayed for the reaction with wild-type and mutated tetraheme subunits, no obvious effects of any of mutated positions on the second-order kinetics were observed under experimental conditions similar to those applied for cytochromes (data not shown).

DISCUSSION

System for Site-Directed Mutagenesis in Bound Cytochrome Subunit and Properties of Obtained Mutants. The genetic experiments previously performed with *Rvi. gelatinosus* cells (*27*, *30*−*32*) indicated that the homologous recombination between chromosomal and plasmid DNA may occur in these cells with the frequency high enough to perform gene substitutions routinely. This prompted us to develop the system targeted on *puf*C in the *puf* operon coding for the RC-bound cytochrome subunit. Such a system based on gene incorporation from the nonreplicative pUC-based pGI7-1 plasmid to a newly constructed ΔC mutant (deletion background) allows us to perform site-specific mutagenesis of the bound cytochrome subunit in the RCs of *Rvi. gelatinosus*.

The ΔC mutant lacking the *puf*C gene on a chromosome can be complemented to the wild-type by single crossover recombination with the pGI7-1 plasmid bearing the original copy of *puf*C, or to RC site-specific mutants by recombination with the pGI7-1 containing a mutated copy of *puf*C. In addition to Southern blot analysis of genomic DNA, the results of gene transfers can be monitored by PCR selectively amplifying the *puf*C gene, and verified by DNA sequence analysis. The expression of RCs with mutated cytochromes can be expected to have the same level as the wild-type since, in each mutant obtained, the copy of *puf*C in the chromosome is always under the control of internal regulatory elements.

Photosynthetic growth of the ΔC deletion background occurs at approximately half the rate of the wild-type cells. A similar situation which was previously observed for the C244 mutant (in which the *puf*C gene was insertionally inactivated) indicated a dispensable, although advantageous role of the *Rvi. gelatinosus* tetraheme subunit in photosynthesis (*30*) and can be explained by the fact that periplasmic electron carriers (HiPIP and cytochrome c_8) are able to directly reduce the photo-oxidized bacteriochlorophyll dimer in the RC core complexes (*35*). All site-specific mutants generated in this study through the complementation of the ΔC deletion background exhibited fast, equal to wild-type growth rates under photosynthetic conditions. Such behavior of the cells can be taken as evidence that all mutated RCs are fully functional in vivo, as expected if the local surface charge substitutions introduced in the bound cytochrome subunit did not alter its overall functional and structural properties when HiPIP was the major electron donor to the RC (*16*).

Interaction Site for Soluble Cytochromes on the Surface of Bound Cytochrome Subunit. Despite uncertainty as to whether the transient electron-transfer complexes between RCs and soluble cytochromes are stabilized by the formation of complementary charged pairs between specific ionized residues located on their encounter surfaces, or rather by the attractions between the domains of complementary delocalized electrostatic potentials (*47*), it has been considered that electrostatic forces play a primary role in controlling these

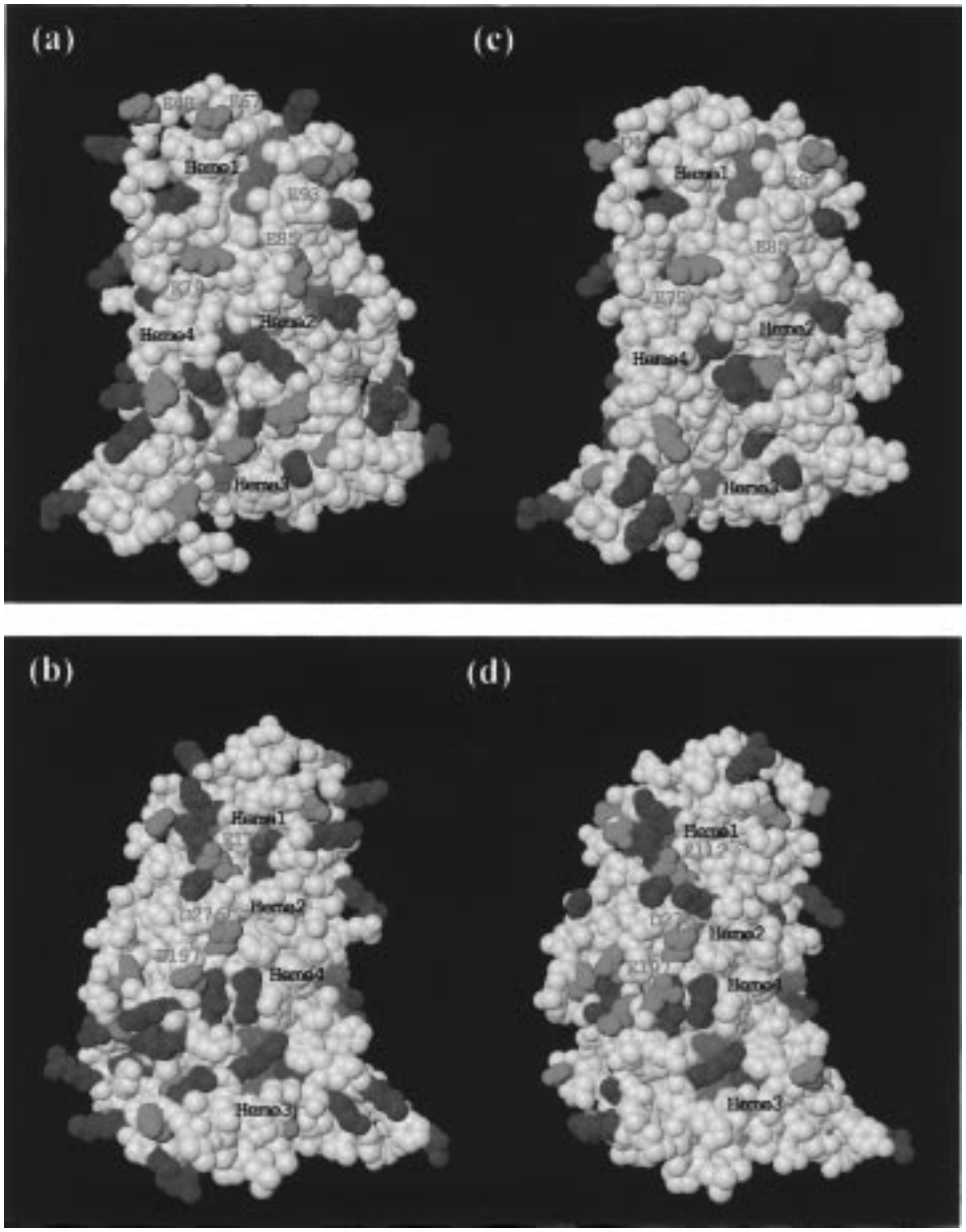

FIGURE 7: Left (top and bottom panel): space-filling representation of the crystallographic structure of the cytochrome subunit of the *Blc. viridis* RC, (a) the orientation of the molecule from which hemes 1 and 2 are the most visible, and (b) the molecule has been rotated with respect to (a) by approximately 180° around the vertical axis. Right (top and bottom panel): the three-dimensional model of the cytochrome subunit of the *Rvi. gelatinosus* RC; (c) and (d) show the same orientations of the molecule as in (a) and (b), respectively. The amino acid residues are colored as follows: Asp, Glu (red); Lys, Arg (blue); others (white). The heme groups are colored green. The distances between the positions of the α-carbon atoms of mutated residues and Fe of heme 1 from the model for *Rvi. gelatinosus* subunit are the following: 20 Å for D46, 12 Å for E79, 13 Å for E85, and 11 Å for E93. The figure was generated by the programs MOLSCRIPT (*74*) and RASTER3D (*75*).

protein−protein interactions. Therefore, the identification of residues directly involved in the process of electrostatic recognition is expected to provide structural information about the configuration of docking complexes and existing binding sites (*48*). The purpose of this study was to map experimentally the specific charged residues of the RC-bound tetraheme subunit which participate in surface recognition of soluble cytochromes for electron transfer.

In the well-characterized complex formed between cytochrome c_2 and *Rba. sphaeroides* RC, electrostatic recognition occurs between lysine residues surrounding the heme crevice of the cytochrome and negatively charged carboxylate groups on the periplasmic surface of the RC (*6, 45, 47, 49*−*51*). A similar mechanism was postulated for the reaction between cytochrome c_2 and a tetraheme subunit bound to the RC of *Blc. viridis*, where the involvement of electrostatic interactions is suggested by the strong ionic strength dependence of the binding (*21, 22*), and inhibitory effects of modification of the lysines of cytochrome c_2 (*23*). Examination of the three-dimensional structure of the *Blc. viridis* tetraheme subunit (Figure 7a,b) shows three areas where the exposed edges of individual hemes are surrounded by negatively charged aspartic or glutamic acids: the vicinities of low-potential heme 1 (*c*-554) or high-potential hemes 2 and 3 (*c*-556 and *c*-559, respectively). As proposed by Knaff et al. (*21*), if structural factors are taken into account, heme 1, despite an unfavorably low redox potential ($E_m = -60$ mV), may provide the most attractive binding site, as it has the

highest degree of surface exposure and the most obvious cluster of surrounding acidic residues (E67, E79, E85, and E93) (Figure 7a). Alternatively, Meyer et al. (*22*) suggested that the cytochrome may directly reduce high-potential heme 2 ($E_m = 310$ mV) if its binding, controlled primarily by E85 and E93, occurs in the region between hemes 1 and 2, or even nearer to heme 2 (Figure 7a). A molecular modeling study (*24*) also showed a third possible binding site located closest to P, high-potential heme 3 ($E_m = 380$ mV) (Figure 7b), although double-flash experiments suggested that this heme is not directly reduced by cytochrome c_2 (*21*).

The high degree of homology between the primary sequences of *Blc. viridis* and *Rvi. gelatinosus* bound tetraheme subunits (*25*) allows us to predict that the overall three-dimensional structures of these proteins are similar. Thus, the structural positions of the individual amino acids of the *Rvi. gelatinosus* tetraheme subunit should approximately correspond to equivalent positions in the *Blc. viridis* structure. This can be visualized by comparison of the space-filling model of the crystallographic structure of *Blc. viridis* tetraheme subunit with the model of *Rvi. gelatinosus* subunit built under the assumption of a similar folding pattern for both proteins (Figure 7, a,b and c,d, respectively). According to the latter model, negatively charged residues on the surface of *Rvi. gelatinosus* tetraheme subunit may form putative docking sites for soluble cytochromes in the same regions as in the case of *Blc. viridis*. Specifically, the acidic cluster around low-potential heme 1 (*c*-551, $E_m = 70 \pm 20$ mV) consists of D46, E79, E85, and E93 (Figure 7c), high-potential heme 2 (*c*-555, $E_m = 300 \pm 20$ mV) is exposed beneath E85 (Figure 7c) and also partially near E112 and D276 (Figure 7d), whereas high-potential heme 3 (*c*-555, $E_m = 320 \pm 30$ mV) is exposed beneath E197 and D276 (Figure 7d).

In the present study, these regions of the *Rvi. gelatinosus* tetraheme subunit were examined by site-directed mutagenesis. The possible involvement of individual acidic residues in the formation of the functional complex with soluble cytochromes was tested by evaluating the effects of their mutational replacements with oppositely charged amino acids. These effects were monitored by measuring the in vitro kinetics of electron transfer between soluble cytochromes and mutated bound cytochrome subunits. Horse mitochondrial cytochrome *c* was employed in most of these assays as an electron donor to the cytochrome subunit since it interacts equally well with both *Blc. viridis* (*21, 22*) and *Rvi. gelatinosus* (*52*) RCs. Furthermore, it has been used as a structural analogue of cytochrome c_2 in several other studies on the interaction sites of soluble cytochromes with RCs and cytochrome bc_1 complexes in other species: *Rba. sphaeroides*, *Rsp. rubrum*, and *Rba. capsulatus* (*23, 49, 50, 53*−*56*).

Significant inhibitory effects on the electron-transfer kinetics with horse cytochrome *c* were observed only for mutants E93K, E79K, E85K, and D46H located near the exposed edge of low-potential heme 1 (Figure 7c). This indicates that the vicinity of heme 1 forms a binding site for soluble cytochromes, in agreement with the proposal of Knaff et al. (*21*). Mutations E93K and E79K, being closest to the exposed edge of this heme (for modeled distances see legend to Figure 7), had the largest inhibitory effect. Inhibition was also observed for the mutation at position 85 (E85K), which, situated between hemes 1 and 2, is still close enough to heme 1 to contribute to the electrostatic interactions at its binding site. The smaller extent of inhibition of E85K as compared to E93K and E79K suggests that the binding of cytochrome *c*, primarily controlled by E93 and E79, occurs closer to heme 1 than to heme 2. A small effect of mutation D46H confirms that the binding site near heme 1 does not overlap that at heme 2, but is rather oriented specifically toward heme 1 (D46 is located somewhat distantly from heme 1 in the opposite direction to heme 2). Consequently, the placement of soluble cytochrome *c* in the area which includes E93, E85, and E79 results in the edge-to-edge distance of about 10 Å between cytochrome *c* heme and heme 1, a distance which is reasonable for immediate electron exchange between these hemes. Accordingly, three acidic groups of E93, E79, and E85 (together with a small contribution of D46) in the interaction domain may be expected to result in a value of a net charge ranging between −3 and −4, which is in good agreement with our estimation for the wild-type cytochrome subunit based upon the ionic strength dependence ($Z_{RC} = -3.6$).

It is noteworthy that the extent in decrease of the rate of re-reduction of cytochrome subunit by horse cytochrome *c* caused by introduction of positive charge at positions E93, E79, E85, and D46 (reflected by the changes in the electrostatic interaction energy and the interaction domain charge) is also consistent with a model assuming the involvement of three or four electrostatic interactions in the binding of cytochrome *c* to the RC. Moreover, double-charge substitutions introduced at E93/E85 and E79/E85, resulting in an additive inhibitory effect, provide further supporting evidence for the proposed site of interaction.

As shown in Figure 7d, the opposite side of the *Rvi. gelatinosus* tetraheme subunit forms the acidic patch consisting of E112, D276, and E197 (conserved also in *Blc. viridis*, Figure 7b), which are located between partially exposed hemes 1 and 2 (E112), and between heme 2 and the more substantially exposed heme 3 (D276, E197). The mutational charge substitutions introduced at these positions (E112K, E197K, and D276H) did not alter the kinetics of electron transfer from soluble cytochrome *c* to the tetraheme subunit indicating that these regions are not involved in the binding and cytochrome *c* apparently reacts at only a single binding site. The vicinity of low-potential heme 4 was excluded from these considerations, since the three-dimensional structure of *Blc. viridis* tetraheme subunit does not show any negatively charged amino acids surrounding the exposed part of its edge.

Cytochrome c_2 from *Blc. viridis* displays considerable amino acid sequence homology and structural similarity to mitochondrial cytochrome *c* (*57*−*60*). In particular, five of six lysine residues surrounding the heme crevice of horse cytochrome *c* are conserved in *Blc. viridis* cytochrome c_2. Moreover, the hydrogen-bonding pattern of *Blc. viridis* cytochrome c_2 seems to be much closer to that of eucaryotic cytochromes *c* than that of other bacterial cytochromes c_2 (*59, 60*). Therefore, *Blc. viridis* cytochrome c_2 is expected to form a complex with the tetraheme subunit in a manner similar to that of mitochondrial cytochrome *c*. Comparable site specificity of the inhibitory effects observed for horse cytochrome *c* and *Blc. viridis* cytochrome c_2 in the reactions with mutated tetraheme subunits indicates that both cyto-

FIGURE 8: Model of possible interaction between the cytochrome subunit of the *Blc. viridis* RC (left) and *Blc. viridis* cytochrome c_2 (right). Thread drawings based on the α-carbon positions are colored white. The side-chain atoms of the charged interacting residues are shown as ball-and-stick models in blue (lysines) and red (glutamates). The heme atoms are also shown as ball-and-stick models in green. The figure was generated using the programs MOLSCRIPT (*74*) and RASTER3D (*75*).

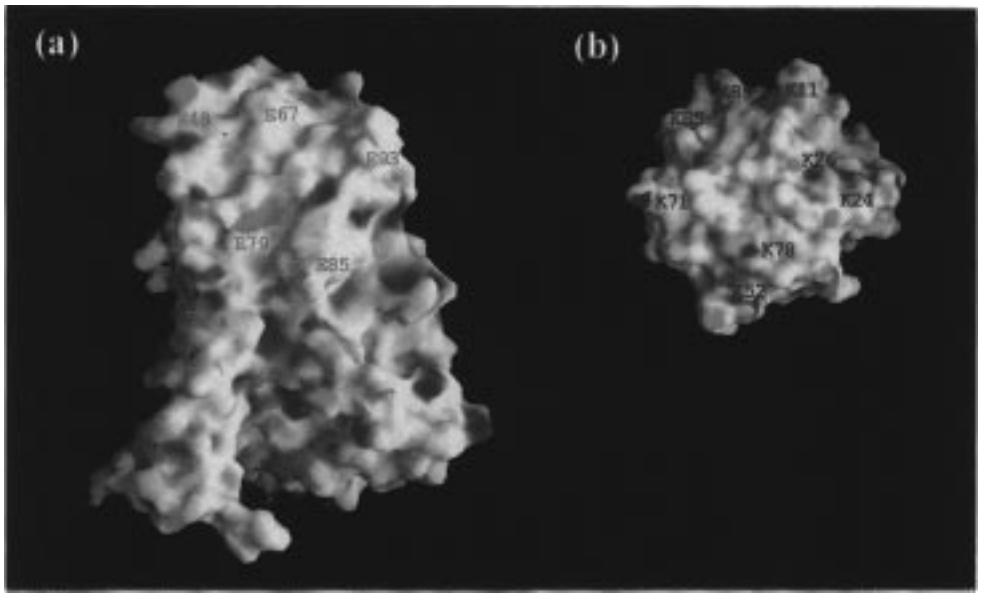

FIGURE 9: Electrostatic potentials mapped onto the surface of the cytochrome subunit of the *Blc. viridis* RC (a) and *Blc. viridis* cytochrome c_2 (b). The orientation of the subunit is the same as in Figure 7a; cytochrome c_2 is viewed from the solvent-exposed heme edge side. The regions with positive and negative potentials are scaled between blue and red, respectively. The figure was generated using the program GRASP (*43*).

chromes recognize the same domain on the surface of the subunit, that is, the vicinity of low-potential heme 1. Since the amino acid sequence in the region around heme 1 of the *Rvi. gelatinosus* tetraheme subunit is highly similar to that of *Blc. viridis*, the cytochrome c_2−RC transient complex for *Blc. viridis* has been modeled (Figure 8). In this model K11, K78, and K71 of cytochrome c_2 interact electrostatically with E67, E79, and E93 in the cytochrome subunit, respectively. Such a configuration of the complex results in approximately parallel orientation of the planes of cytochrome *c* heme and heme 1 of the subunit with the 10 Å edge-to-edge distance between them. The model seems also to be consistent with delocalized electrostatic potentials of the proposed interacting surfaces. As shown in Figure 9, the area of strong negative potential in the region including E79, E93, E67, and E48 of the subunit complements the dominantly positive encounter surface surrounding the heme crevice of cytochrome c_2. The number of charged residues participating in the binding correlates with the experimental estimations reported for the reaction of *Blc. viridis* cytochrome c_2 with *Blc. viridis* RCs (the number of 3.5 (*21*) or 2.5 (*22*) interacting charge pairs was obtained from the ionic strength dependence of this reaction). Additionally, as suggested from our kinetic results, other charged residues in this region (particularly E85 and E48, in analogy to D46 of *Rvi. gelatinosus*) may be also expected to contribute to the binding. One may also note

that only two out of three acidic residues proposed to form the *Blc. viridis* binding site are conserved in *Rvi. gelatinosus* (E79 and E93). The lack of E67, which is not compensated by other negatively charged residues on the immediate left to heme 1 (Figure 7c), may account for the lower efficiency of *Blc. viridis* cytochrome c_2 in reduction of the *Rvi. gelatinosus* tetraheme subunit when compared to its reactivity with the physiological partner, the *Blc. viridis* tetraheme subunit (*21, 22*). Finally, it should be emphasized that the proposed configuration of the complex requires further experimental verification, and cannot be considered to be unique, since the assignment of interacting residues is restricted by the lack of information about the conformational changes that may occur when cytochrome c_2 approaches and binds to the RC. Furthermore, it is possible that cytochrome c_2 may adopt more than one specific orientation with respect to the bound cytochrome.

In *Rvi. gelatinosus*, cytochrome c_2 is functionally replaced by HiPIP, which mediates the electron transfer between the cytochrome bc_1 complex and the RC (*16*). Soluble cytochrome *c*-551 (with reported values of its redox potential; $E_m = 28$ (*61*), 50 (*35*), or even 294 mV (*62*)) belonging to the cytochrome c_8 family was also found to efficiently re-reduce photo-oxidized tetraheme subunit (*35*). A similar situation exists in two other species from the β-subclass containing HiPIP and cytochrome c_8 in the soluble fraction instead of cytochrome c_2: *Rfx. fermentans* (*18*−*20*) and *Rcy. tenuis* (*17*). Our kinetic results with mutated tetraheme subunits indicate that *Rvi. gelatinosus* cytochrome c_8 binds to the RC in the same region on the surface of the subunit as other soluble cytochromes. Although mutations located near the exposed edge of heme 1 had inhibitory effects on the rate of electron transfer from cytochrome c_8, the extent of inhibition caused by individual mutations was less pronounced when compared with respective inhibitory effects observed for horse cytochrome *c* and *Blc. viridis* cytochrome c_2. This suggests that in the binding of cytochrome c_8 to the RC less charge is involved, or factors other than electrostatics may play a more dominant role. The structural properties of cytochrome c_8 may account for this situation. Cytochromes c_8 related to *Pseudomonas* cytochrome *c*-551 (*63, 64*) are smaller in size than cytochromes c_2, and display a less asymmetric charge distribution on their encounter surface (*47, 65*).

In contrast to the kinetic behavior of soluble cytochromes, the interaction of *Rvi. gelatinosus* HiPIP with RCs was not influenced by any of the mutated positions examined in this study to the extent that would allow us to identify its binding site. Thus, it is possible that HiPIP recognizes a different site on the RC than soluble cytochromes, or that the mode of interaction in this case is different. It is noteworthy that HiPIPs are generally very poor electron donors to the RCs from *Blc. viridis* (*22*), a species that possesses only cytochrome c_2 in the soluble periplasmic fraction. Therefore, we may expect that the tetraheme subunit of *Rvi. gelatinosus* has some structural characteristics that allow an efficient electron transfer from HiPIP. Further experiments to clarify the interaction of this protein with the RC employing site-directed mutants of the tetraheme subunit are currently in progress.

Functional Significance of Low-Potential Heme 1 of Bound Cytochrome Subunit. The redox midpoint potentials of individual hemes within the tetraheme subunit vary depending on the species; however the linear geometry of their arrangement seems to be conserved and to follow the order determined for *Blc. viridis*, that is, high-low-high-low potential with the first high- and last low-potential hemes closest and most distant from the special pair of bacteriochlorophyll (P), respectively (*14*). The consensus on the role of the high-potential hemes is that their photo-oxidation is followed by re-reduction processes, in which soluble electron carriers participate to complete light-induced cyclic electron transfer (*15*). It has been clearly established that the first high-potential heme 3 (lying closest to P) is capable of direct electron donation to P^+. Photo-oxidation of the second high-potential heme 2 via heme 3 as well as the possible involvement of low-potential heme 4 (interpositioned between two high-potential hemes 2 and 3) in the reduction of P^+ has also been observed (*66*−*70*). However, no clear role can be yet assigned to the low-potential hemes, and the sequence of electron flow through all four hemes toward P^+ remains unknown.

A recent comparison between the available amino acid sequences of various tetraheme subunits strongly suggests that the surface environment of the low-potential heme 1, most distant from P, is structurally conserved and characterized by the presence of a cluster of acidic residues surrounding the exposed part of its edge (*38*) (*Acidiphilum rubrum* is an exception (*71*)). As shown by the present study, this cluster of negative charges recognizes a basic surface of soluble cytochromes and forms a binding site for them. Therefore, the electrostatic surface around heme 1 seems to play a primary role in the formation of the functional complex between the tetraheme subunit and soluble cytochromes. Considering the distance between the donor and the acceptor as a dominant factor for the rate of electron transfer (*72*), heme 1 should directly accept electrons carried by soluble cytochromes. The resulting electron flow from high- to low-potential heme (in the case of interaction with high-potential cytochromes) will be in striking contradiction to the general considerations of redox-potential-driven electron transfer. However, it may provide one possible explanation for the lack of correlation between the driving force and rate constants observed for the electron transfer from different soluble cytochromes to *Blc. viridis* tetraheme subunit (*22*).

The subsequent steps of electron transfer within the tetraheme subunit can be reasonably postulated. Most probably heme 1 will reduce neighboring high-potential heme 2 (*21*), although the possibility of direct electron exchange between two low-potential hemes cannot be fully ruled out. To date, despite extensive studies on electron flow from cytochrome hemes to P^+, there is no data (mainly due to experimental limits) describing the contribution of heme 1. However, if heme 1 is the first heme to be reduced by soluble cytochrome, all four hemes of the subunit are likely to be involved in the electron transfer toward P^+.

If one accepts the functional importance of the interposition of the second low-potential heme 4 between two high-potential hemes (*73*), an equivalent role may be assigned for the outermost low-potential heme 1, which upon binding of soluble high-potential cytochromes will be placed between two high-potential hemes. The effect of the driving force on the electron transfer in this system remains to be

elucidated. In general, physiological partners of the tetraheme cytochrome subunits have E_m values (ranging from 240 to 400 mV for cytochromes c_2 and c_8 and HiPIPs) similar to those of the high-potential hemes of the subunit. In this respect, the existence of the binding site on RC formed by the low-potential heme 1 is not consistent with the general idea of "downhill" redox-potential-driven electron transfer and seems to indicate that purple bacterial tetraheme systems operate in more refined way, which is still far from being understood.

In the present study, the involvement of specific negatively charged residues of the RC-bound tetraheme subunit in the formation of a functional complex with soluble cytochromes was demonstrated through site-specific mutagenesis. The identification of the binding domain in the vicinity of low-potential heme 1 provided the first experimental indication for its involvement in electron flow from soluble cytochromes to P^+. It is anticipated that future mutations in the *Rvi. gelatinosus* RC-bound cytochrome subunit will provide further insights into how all four hemes function in this electron-transfer pathway.

REFERENCES

1. Hiraishi, A. (1997) *Int. J. Syst. Bacteriol. 47*, 217−219.
2. Deisenhofer, J., Epp, O., Miki, K., Huber, R., and Michel, H. (1985) *Nature 318*, 618−624.
3. Deisenhofer, J., and Michel, H. (1989) *EMBO J. 8*, 2149−2170.
4. Deisenhofer, J., Epp, O., Sinning, I., and Michel, H. (1995) *J. Mol. Biol. 246*, 429−457.
5. Allen, J. P., Feher, G., Yeates, T. O., Komiya, H., and Rees, D. C. (1987) *Proc. Natl. Acad. Sci. U.S.A. 84*, 5730−5734.
6. Allen, J. P., Feher, G., Yeates, T. O., Komiya, H., and Rees, D. C. (1987) *Proc. Natl. Acad. Sci. U.S.A. 84*, 6162−6166.
7. Chang, C. H., Tiede, D., Tang, J., Smith, U., Norris, J., and Schiffer, M. (1986) *FEBS Lett. 205*, 82−86.
8. Coleman, W. J., and Youvan, D. C. (1990) *Annu. Rev. Biophys. Biophys. Chem. 19*, 333−367.
9. Diner, B. A., Nixon, P. J., and Farchaus, J. W. (1991) *Curr. Opin. Struct. Biol. 1*, 546−554.
10. Lau*β*ermair, E., and Oesterhelt, D. (1992) *EMBO J. 11*, 777−783.
11. Bibikova, M., Arlt, T., Zinth, W., and Oesterhelt, D. (1995) in *Photosynthesis: from Light to Biosphere* (Mathis, P., Ed.) Vol I, pp 867−870, Kluwer Academic, Dordrecht, The Netherlands.
12. Dohse, B., Mathis, P., Wachtveitl, J., Laussermair, E., Iwata, S., Michel, H., and Oesterhelt, D. (1995) *Biochemistry 34*, 11335−11343.
13. Arlt, T., Dohse, B., Schmidt, S., Wachtveitl, J., Laussermair, E., Zinth, W., and Oesterhelt, D. (1996) *Biochemistry 35*, 9235−9244.
14. Nitschke, W., and Dracheva, S. M. (1995) in *Anoxygenic Photosynthetic Bacteria* (Blankenship, R. E., Madigan, M. T., and Bauer, C. E., Eds.) pp 775−805, Kluwer Academic, Dordrecht, The Netherlands.
15. Meyer, T. E., and Donohue, T. J. (1995) in *Anoxygenic Photosynthetic Bacteria* (Blankenship, R. E., Madigan, M. T., and Bauer, C. E., Eds.) pp 725−745, Kluwer Academic, Dordrecht, The Netherlands.
16. Schoepp, B., Parot, P., Menin, L., Gaillard, J., Richaud, P., and Verméglio, A. (1995) *Biochemistry 34*, 11736−11742.
17. Menin, L., Schoepp, B., Parot, P., and Verméglio, A. (1997) *Biochemistry 36*, 12183−12188.
18. Hochkoeppler, A., Ciurli, S., Venturoli, G., and Zannoni, D. (1995) *FEBS Lett. 357*, 70−74.
19. Hochkoeppler, A., Zannoni, D., Ciurli, S., Meyer, T. E., Cusanovich, M. A., and Tollin, G. (1996) *Proc. Natl. Acad. Sci. U.S.A. 93*, 6998−7002.
20. Hochkoeppler, A., Ciurli, S., Kofod, P., Venturoli, G., and Zannoni, D. (1997) *Photosynth. Res. 53*, 13-21.
21. Knaff, D. B., Willie, A., Long, J. E., Kriauciunas, A., Durham, B., and Millett, F. (1991) *Biochemistry 30*, 1303−1310.
22. Meyer, T. E., Bartsch, R. G., Cusanovich, M. A., and Tollin, G. (1993) *Biochemistry 32*, 4719−4726.
23. Güner, S., Willie, A., Millett, F., Caffrey, M. S., Cusanovich, M. A., Robertson, D. E., and Knaff, D. B. (1993) *Biochemistry 32*, 4793−4800.
24. Sogabe, S., Saeda, M., Uno, A., Ezoe, T., Miki, M., Matsuura, Y., Matsuura, K., and Miki, K. (1992) in *Research in Photosynthesis* (Murata, N., Ed.) Vol. II, pp 531−534, Kluwer Academic, Dordrecht, The Netherlands.
25. Nagashima, K. V. P., Matsuura, K., Ohyama, S., and Shimada, K. (1994) *J. Biol. Chem. 269*, 2477−2484.
26. Ouchane, S., Picaud, M., and Astier, C. (1995) *FEBS Lett. 374*, 130−134.
27. Ouchane, S., Picaud, M., Reiss-Husson, F., Vernotte, C., and Astier, C. (1996) *Mol. Gen. Genet. 252*, 379−385.
28. Fukushima, A., Matsuura, K., Shimada, K., and Satoh, T. (1988) *Biochim. Biophys. Acta 933*, 399−405.
29. Nitschke, W., Agalidis, I., and Rutherford, A. W. (1992) *Biochim. Biophys. Acta 1100*, 49−57.
30. Nagashima, K. V. P., Shimada, K., and Matsuura, K. (1996) *FEBS Lett. 385*, 209−213.
31. Ouchane, S., Picaud, M., Vernotte, C., Reiss-Husson, F., and Astier, C. (1997) *J. Biol. Chem. 272*, 1670−1676.
32. Ouchane, S., Picaud, M., Vernotte, C., and Astier, C. (1997) *EMBO J. 16*, 4777−4787.
33. Saeki, K., Suetsugu, Y., Tokuda, K., Miyatake, Y., Young, D. A., Marrs, B. L., and Matsubara, H. (1991) *J. Biol. Chem. 266*, 12889−12895.
34. Sambrook, J., Fritsch, E. F., and Maniatis, T. (1989) in *Molecular Cloning: A Laboratory Manual*, 2nd ed., Cold Spring Harbor Laboratory Press, Cold Spring Harbor, NY.
35. Osyczka, A., Yoshida, M., Nagashima, K. V. P., Shimada, K., and Matsuura, K. (1997) *Biochim. Biophys. Acta 1321*, 93−99.
36. Bartsch, R. G. (1978) in *The Photosynthetic Bacteria* (Clayton, R. K., and Sistrom, W. R., Eds.) pp 249−279, Plenum Press, New York and London.
37. Matsuura, K., and Shimada, K. (1986) *Biochim. Biophys. Acta 852*, 9−18.
38. Nagashima, K. V. P., Sakuragi, Y., Shimada, K., and Matsuura, K. (1998) *Photosynth. Res*. (in press).
39. Kleywegt, G. J. (1996) *CCP4/ESF-EACBM Newsletter on Protein Crystallography 32*, 32−36.
40. Kleywegt, G. J., and Jones, T. A. (1997) *Methods Enzymol. 277*, 208−230.
41. Brünger, A. T. (1992) *X-PLOR, A System for Crystallography and NMR*, Yale University Press, New Haven, CT.
42. Laskowski, R. A., MacArthur, M. W., Moss, D. S., and Thornton, J. M. (1993) *J. Appl. Crystallogr. 26*, 283−291.
43. Nicholls, A., Sharp, K. A., and Honig, B. H. (1991) *Proteins 11*, 281−296.
44. Watkins, J. A., Cusanovich, M. A., Meyer, T. E., and Tollin, G. (1994) *Protein Sci. 3*, 2104−2114.
45. Caffrey, M. S., Bartsch, R. G., and Cusanovich, M. A. (1992) *J. Biol. Chem. 267*, 6317−6321.
46. Tollin, G., Cheddar, G., Watkins, J. A., Meyer, T. E., and Cusanovich, M. A. (1984) *Biochemistry 23*, 6345−6349.
47. Tiede, D. M., Vashishta, A. C., and Gunner, M. R. (1993) *Biochemistry 32*, 4515−4531.
48. Meyer, T. E., Tollin, G., and Cusanovich, M. A. (1994) *Biochimie 76*, 480−488.
49. Hall, J., Zha, X., Durham, B., O′Brien, P., Vieira, B., Davis, D., Okamura, M., and Millett, F. (1987) *Biochemistry 26*, 4494−4500.
50. Long, J. E., Durham, B., Okamura, M., and Millett, F. (1989) *Biochemistry 28*, 6970−6974.
51. Adir, N., Axelrod, H. L., Beroza, P., Isaacson, R. A., Rongey, S. H., Okamura, M. Y., and Feher, G. (1996) *Biochemistry 35*, 2535−2547.

52. Matsuura, K., Fukushima, A., Shimada, K., and Satoh, T. (1988) *FEBS Lett. 237*, 21−25.
53. Hall, J., Zha, X., Yu, L., Yu, C. A., and Millett, F. (1987) *Biochemistry 26*, 4501−4504.
54. Hall, J., Ayres, M., Zha, X., O′Brien, P., Durham, B., Knaff, D. B., and Millett, F. (1987) *J. Biol. Chem. 262*, 11046−11051.
55. Hall, J., Kriaucionas, A., Knaff, D. B., and Millett, F. (1987) *J. Biol. Chem. 262*, 14005−14009.
56. Van der Wal, H. N., Van Grondelle, R., Millett, F., and Knaff, D. B. (1987) *Biochim. Biophys. Acta 893*, 490−498.
57. Ambler, R. P., Meyer, T. E., and Kamen, M. D. (1976*) Proc. Natl. Acad. Sci. U.S.A. 73*, 472−475.
58. Ambler, R. P., Daniel, M., Hermoso, J., Meyer, T. E., Bartsch, R. G., and Kamen, M. D. (1979) *Nature 278*, 659−660.
59. Sogabe, S., Ezoe, T., Kasai, N., Saeda, M., Uno, A., Miki, M., and Miki, K. (1994) *FEBS Lett. 345*, 5−8.
60. Sogabe, S., and Miki, K. (1995) *J. Mol. Biol. 252*, 235−247.
61. Meyer, T. E., Przysiecki, C. T., Watkins, J. A., Bhattacharyya, A., Simondsen, R. P., Cusanovich, M. A., and Tollin, G. (1983) *Proc. Natl. Acad. Sci. U.S.A. 80*, 6740−6744.
62. Borsari, M., Benini, S., Marchesi, D., and Ciurli, S. (1997) *Inorg. Chim. Acta 263*, 379−384.
63. Ambler, R. P., Meyer, T. E., and Kamen, M. D. (1979) *Nature 278*, 661−662.
64. Ambler, R. P. (1991) *Biochim. Biophys. Acta 1058*, 42−47.
65. Samyn, B., De Smet, L., Van Driessche, G., Meyer, T. E., Bartsch, R. G., Cusanovich, M. A., and Van Beeumen, J. J. (1996) *Eur. J. Biochem. 236*, 689−696.
66. Holten, D., Windsor, M. W., Parson, W. W., and Thornber, J. P. (1978) *Biochim. Biophys. Acta 501*, 112−126.
67. Schopes, R. J., Levine, L. M. A., Holten, D., and Wraight, C. A. (1987) *Photosynth. Res. 12*, 165−180.
68. Dracheva, S. M., Drachev, L. A., Konstantinov, A. A., Semenov, A. Y., Skulachev, V. P., Arutjunjan, A. M., Shuvalov, V. A., and Zaberezhnaya, S. M. (1988) *Eur. J. Biochem. 171*, 253−264.
69. Ortega, J. M., and Mathis, P. (1992) *FEBS Lett. 301*, 45−48.
70. Ortega, J. M., and Mathis, P. (1993) *Biochemistry 32*, 1141−1151.
71. Nagashima, K. V. P., Matsuura, K., Wakao, N., Hiraishi, A., and Shimada, K. (1997) *Plant Cell Physiol. 38*, 1249−1258.
72. Moser, C. C., Keske, J. M., Warncke, K., Farid, R. S., and Dutton, P. L. (1992) *Nature 355*, 796−802.
73. Nitschke, W., and Rutherford, A. W. (1994) *Biochem. Soc. Trans. 22*, 694−699.
74. Kraus, P. (1991) *J. Appl. Crystallogr. 24*, 946−950.
75. Merritt, E. A., and Murphy, M. E. P. (1997) *Acta Crystallogr., Sect. D 50*, 869−873.

BI980910H